Asia-Pac. J. Atmos. Sci., 53(1), 121-130, 2017
DOI:10.1007/s13143-017-0010-y

pISSN 1976-7633 / eISSN 1976-7951

UAH Version 6 Global Satellite Temperature Products: Methodology and Results

Roy W. Spencer, John R. Christy, and William D. Braswell

Earth System Science Center, University of Alabama in Huntsville, Huntsville, Alabama, USA

(Manuscript received 26 February 2016; accepted 1 November 2016)

Abstract: Version 6 of the UAH MSU/AMSU global satellite temperature dataset represents an extensive revision of the procedures employed in previous versions of the UAH datasets. The two most significant results from an end-user perspective are (1) a decrease in the global-average lower tropospheric temperature (LT) trend from +0.14°C decade^{-1} to +0.11°C decade^{-1} (Jan. 1979 through Dec. 2015); and (2) the geographic distribution of the LT trends, including higher spatial resolution, owing to a new method for computing LT. We describe the major changes in processing strategy, including a new method for monthly gridpoint averaging which uses all of the footprint data yet eliminates the need for limb correction; a new multi-channel (rather than multi-angle) method for computing the lower tropospheric (LT) temperature product which requires an additional tropopause (TP) channel to be used; and a new empirical method for diurnal drift correction. We show results for LT, the mid-troposphere (MT, from MSU2/AMSU5), and lower stratosphere (LS, from MSU4/AMSU9). A 0.03°C decade^{-1} reduction in the global LT trend from the Version 5.6 product is partly due to lesser sensitivity of the new LT to land surface skin temperature (est. 0.01°C decade^{-1}), with the remainder of the reduction (0.02°C decade^{-1}) due to the new diurnal drift adjustment, the more robust method of LT calculation, and other changes in processing procedures.

Key words: Global temperature, satellites, climate change

1. Background and overview

The global coverage by polar-orbiting satellites provides an attractive vantage point from which to monitor climate variability and change. Average air temperature over relatively deep atmospheric layers can be monitored, with minimum cloud contamination, using passive microwave radiometers operating in the 50-60 GHz range which measure thermal microwave emission from molecular oxygen that is proportional to temperature. The temperature of such bulk atmospheric layers relate directly to heat content and thus to the rate at which heat may be accumulating in the atmosphere due to enhanced greenhouse gas forcing and other climate changes. The Microwave Sounding Units (MSUs) and the Advanced Microwave Sounding Units (AMSUs) have served primarily the numerical weather prediction modelling community for over thirty years. That these instruments are stable enough to provide a climate monitoring capability of the bulk troposphere was first demonstrated by Spencer and Christy (1990), and verified by Mears et al. (2003), producing the "UAH (University of Alabama in Huntsville)" and "RSS (Remote Sensing System)" datasets, respectively.

The brightness temperatures (T_b) of three primary layers are monitored: the lower troposphere (LT), mid-troposphere (MT), and lower stratosphere (LS, Spencer and Christy, 1993), nomenclature which refers to the layer of peak sensitivity. Additionally, we now produce a tropopause (TP) channel product, which in combination with MT and LS is used to calculate a revised LT product. MT is computed from MSU channel 2 (MSU2) or AMSU channel 5 (AMSU5); TP is computed from MSU3 or AMSU7; and LS is computed from MSU4 or AMSU9.

The period of operation of the MSUs was from late 1978 to the early 2000s, while the AMSUs have been operating since late 1998. The ascending node time and periods of operation of the various satellites used in the UAH Version 6 dataset are shown in Fig. 1. We will refer to the satellites beginning their operation with ascending nodes around 19:30 as "7:30" satellites, and those starting from 13:30 to 15:00 as "1:30" satellites.

Since the early days of the global satellite temperature monitoring efforts, adjustments to the data have been necessary. Satellites must be intercalibrated during overlapping periods of operation due to differences in absolute calibration of a few tenths of a degree C. Furthermore, slow decay of the orbit altitude causes the multi-view angle method of lower troposphere (LT) temperature retrievals (Wentz and Schabel, 1998) to become biased cold, and a dependence of the calibrated MSU measurements on the instrument temperature (Christy et al., 2000) causes a spurious warming of the T_b over time. Corrections for such effects can either be well understood and straightforward, such as the orbit decay correction which is based upon satellite instrument scan geometry and average tropospheric temperature lapse rates; or poorly understood and empirical, such as the instrument temperature effect which is quantified by comparing data from simultaneously operating satellites. These effects have been adjusted for in both the RSS and UAH datasets for many years. Finally, orbit decay also causes most of the satellites to drift in their local time of observation, requiring a diurnal drift correction, which can be done either empirically or with diurnal cycle information from a climate model.

Corresponding Author: Roy W. Spencer, Earth System Science Center, University of Alabama in Huntsville, 320 Sparkman Drive, Huntsville, Alabama 35805, USA.
E-mail: roy.spencer@nsstc.uah.edu

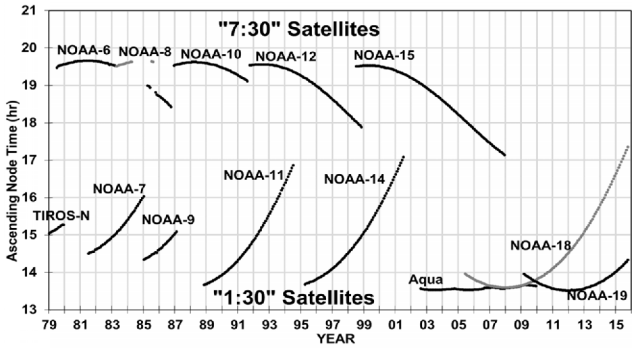

Fig. 1. Local ascending node times for all satellites during their valid date ranges used in Version 6 processing. We do not use NOAA-17 (short record), Metop (failed AMSU7), NOAA-16 (excessive calibration drifts), NOAA-14 after July, 2001 (excessive calibration drift), NOAA-9 after Feb. 1987 for MSU2 only (failed channel), or NOAA-15 after 2007 (calibration drift in AMSU5).

In Version 6 of the UAH global temperature products, almost all of the dataset correction and processing procedures have been improved. We mention two of them here as they represent a major departure from past practices.

Firstly, the calculation of gridpoint data from cross-track through-nadir scanners must address the fact that the different satellite view angles produce 'limb darkening', that is, they measure slightly different altitudes in the atmosphere leading to different T_b. This is often handled with limb corrections (Spencer and Christy, 1992a) as an initial processing step. Limb corrections from the MSU are not very precise from the standpoint of producing the same weighting function profile of temperature sensitivity, owing to a limited number of overlapping channels' weighting functions which when linearly combined cannot accurately reproduce, say, the nadir weighting function (e.g. Conrath, 1972). The AMSUs enable somewhat more accurate limb corrections due to more available overlapping channels, but using all of those channels routinely would require them to be fully functioning over the entire period of record, which is seldom the case. In Version 6 we avoid multi-channel limb corrections by computing monthly gridpoint averages for a given channel at each of the different satellite view angles separately, then statistically estimating from those the T_b at an intermediate "reference" Earth incidence angle T_b. In this way, all of the different view angles' data are still included, but limb corrections are not required.

The second change of major importance is the methodology for computing the lower tropospheric (LT) temperature product, which has previously been computed as a weighted difference between different view angles (Spencer and Christy, 1992b). While the previous method has been sufficient for global and hemispheric average calculations, it is not well suited to gridpoint calculations in an era when regional -- rather than just global -- climate change is becoming of more interest. This is because the previous LT calculation required, and therefore represented, an entire scan line which has a length of approximately 2,000 km. It also included an inherent assumption that the same air mass and underlying surface was being sampled by the various view angles in a single scan. Thus, since LT was based upon a weighted difference of different view angles (and thus different locations), departures from airmass or surface uniformity along the scan lead to errors in the resulting LT calculation for that scan line. We have devised a new method for computing LT involving a multi-channel retrieval, rather than a multi-view angle retrieval, using only data from the same geographic location (gridpoint) which avoids the errors which arise from this peculiar spatial sampling.

2. Pre-processing calculations

a. Reference Earth incidence angles

Since through-nadir scanning temperature sounders are sensitive to different altitudes at the different view angles, in previous analyses either limb corrections have been performed or a restricted range of near-nadir data have been used for climate monitoring. We depart from these practices by using T_b at all of the different view angles measured at a gridpoint location in a given month to statistically estimate the T_b at a reference Earth incidence angle. We have found sampling noise in the latitude zones of frequent baroclinic wave activity is minimized by using an intermediate reference earth incidence angle (neither near-nadir nor near-limb) which then provides 28 almost-evenly spaced samples longitudinally around the Earth in a day (ascending or descending passes). If either nadir or limb positions are used, then there are approximately only 14 samples around the Earth.

Through experimentation with which reference angle provided the least sampling noise in the resulting monthly fields, we decided on MSU print positions 4 and 8, which correspond to an Earth incidence angle of 21.59 deg. at the equator for the NOAA-14 satellite during January 1996. This reference angle is then used for MT, TP, LS from MSU and their eventual combination into the LT product from the MSU instruments.

Because the AMSU has slightly different channel characteristics than MSU, its atmospheric weighting functions are slightly different; for example AMSU channel 5 peaks lower in altitude than does MSU channel 2. We account for this difference by determining an Earth incidence angle from AMSU whose resulting weighting function closely matches the corresponding MSU channel weighting function at its reference Earth incidence angle, based upon radiative transfer theory. The resulting reference Earth incidence angles are 34.99 deg. (initially) for AMSU5, 13.18 deg. for AMSU7, and 36.31 deg. for AMSU9, values which were calculated at the equator from NOAA-15 in January 1999.

Unfortunately, the theoretically-based AMSU5 reference incidence angle of 34.99 deg. was found to cause the resulting LT and MT trends, after all processing described below was completed, to be anomalously cold at very high terrain altitudes, especially over the Greenland ice sheet and the Himalayas compared to surrounding low-elevation areas. This

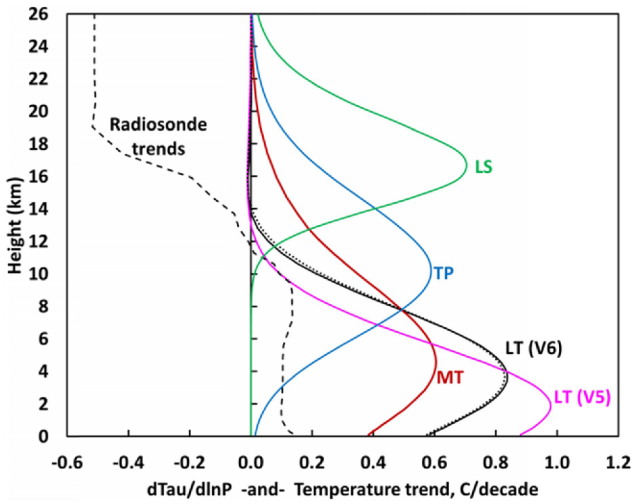

Fig. 2. MSU weighting functions computed from radiative transfer theory for the chosen reference Earth incidence angles, and the resulting LT averaging kernels computed from a linear combination of the MT, TP, and LS weighting functions (the dotted line is for LT computed from AMSU). Also shown is an estimate of the global temperature trend profile (dashed) from the average of RAOBCORE and RATPAC radiosonde data used to determine the stratospheric sensitivity of the new LT averaging kernel.

problem was traced to a probable error in the theoretically calculated AMSU5 weighting function, which apparently peaks slightly lower in altitude than the theory suggests, causing a mismatch between the early MSU measurements and the later AMSU measurements. To correct for this, we increased the AMSU5 reference Earth incidence angle by small amounts until the spurious effect on gridpoint trends over Greenland and the Himalayas was largely eliminated. The adjusted AMSU5 reference Earth incidence angle is 38.31 deg., an increase of about 3.3 deg. This change did not affect the global temperature trends at the 0.01 deg. °C decade^{-1} level, but it did reduce the average land trends and increase the average ocean trends in LT and MT. As we shall see in Section 7, it also resulted in much better continuity of gridpoint tropospheric temperature trends across land-ocean boundaries. It should be noted that this MSU/AMSU weighting function mismatch problem might have been handled by intercalibration of satellites over land and ocean separately, but our experiments with this led to an unacceptably large amount of noise in the gridpoint LT trends.

b. Multi-channel LT averaging kernel

The computation of a new multi-channel averaging kernel for the LT product uses a linear combination of the MT, TP, and LS channels to maximize sensitivity to the lower troposphere while minimizing sensitivity to the lower stratosphere. The result is shown in Fig. 2, for both the MSU and AMSU LT averaging kernels. The LT computation is a linear combination of MSU2, 3, 4 or AMSU5, 7, 9 (MT, TP, LS):

$$\mathrm{LT} = a_1\mathrm{MT} + a_2\mathrm{TP} + a_3\mathrm{LS}, \quad (1)$$

where $a_1 = 1.538$, $a_2 = -0.548$, and $a_3 = 0.01$. As seen in Fig. 2, the new multi-channel LT weighting function is located somewhat higher in altitude than the old LT weighting function, which could make it sensitive to cooling in the lower stratosphere that might potentially mask global warming effects (Fu et al., 2004). To quantify this, we applied the old and new LT weighting functions in Fig. 2 to the vertical profile of average global temperature trends from two radiosonde datasets, RATPAC (Free and Seidel, 2005) and RAOBCORE (Haimberger, 2007), also shown in Fig. 2. The resulting net difference between old and new LT trends is small, less than 0.01°C decade^{-1}. This is because the slightly greater sensitivity of the new LT weighting profile to stratospheric cooling is cancelled by greater sensitivity to enhanced upper tropospheric warming, compared to the old LT profile.

3. MSU and AMSU calibration

a. MSU calibration

The MSU calibration is a linear interpolation of the Earth-view radiometer digital count data between the deep-space radiometer digital counts (assumed viewing 2.7 K) and the radiometer counts when viewing the on-board warm calibration target, at temperature, T_w, yielding the initial calibrated brightness temperature, T_{b0}. Our experiments with alternative calibration strategies have yielded mixed results when comparing co-orbiting satellites, and so a simple two-point linear calibration method has been retained.

Then, because of a still unexplained dependence of that calibrated T_{b0} on T_w (Christy et al., 2000) an empirical instrument body temperature correction is made,

$$T_b = T_{b0} - \beta(T_w - T_{w0}), \quad (2)$$

where $T_{w0} = 280$ K is the approximate average value of T_w across all MSU instruments; its precise value does not affect the final computation of the temperature anomaly products, and is included to keep the calibrated T_b within realistic ranges.

An example of this instrument temperature dependence is shown in Fig. 3 for MSU channel 2 on the NOAA-12 and NOAA-14 satellites during their four-year overlap, where the instrument temperature refers to the warm calibration target temperature T_w. Only ocean data in the equator to 10°N latitude band were used in Fig. 3, with each data point being a monthly average. In Fig. 3a, an obvious difference between the two satellites' T_{b0} is seen which is strongly correlated with the two instruments' warm target temperature difference. The time series of the difference in T_{b0} is then regressed against the warm target temperatures in order to get regression coefficients that mostly remove the effect, seen in Fig. 3b. Clearly, without removal of this effect there would be a significant spurious trend in the calibrated T_b from MSU as the satellites drifted

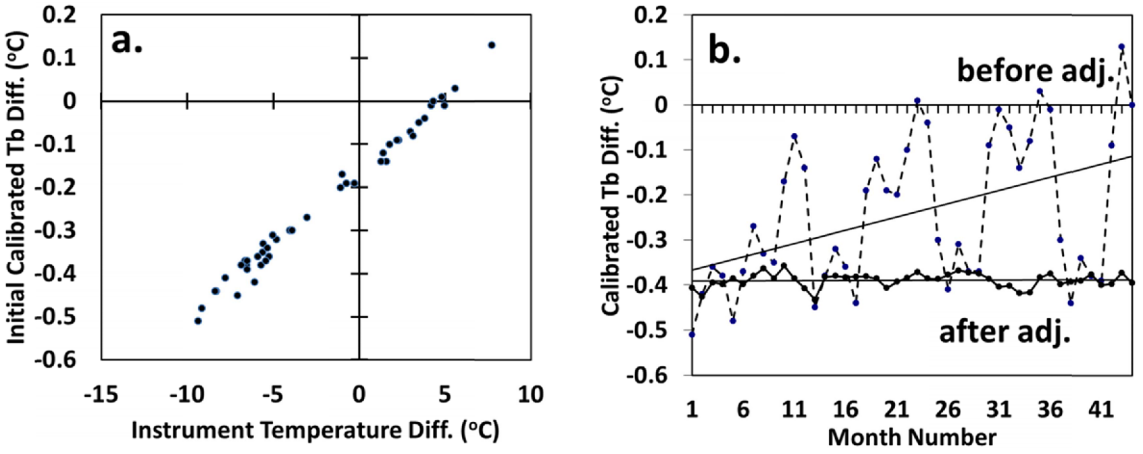

Fig. 3. (a) Difference between NOAA-12 and NOAA-14 MSU2 monthly average T_b over the tropical oceans during their four-year overlap plotted against those instruments' calibration target temperatures, T_w; (b) time series of the T_b difference in (a) before and after removal of the T_w dependence.

toward different local observation times and warmer instrument temperatures, illustrating the necessity of the adjustment.

Similar regressions were performed for MSU2, 3, and 4 using 20°N-20°S ocean-only data during overlaps in operations between satellites. The overlap with Tiros-N was not long enough to obtain a good regression estimate, and so that satellite had values assigned based upon averaging the other 1:30 satellite results. The resulting target coefficient β values used are shown in Table 1, which indicate, in general, several percent crosstalk between instrument temperature and calibrated brightness temperature.

The reason for the target temperature dependence is not yet known with any certainty, but might be related to a dependence of the radiometer local oscillator frequency (and thus weighting function height) on instrument temperature (Lu and Bell, 2014). We note that the β value for NOAA-9 MSU2 (0.032) is now much lower than our previous value used in Version 5 (0.058), and consistent with the other satellites, alleviating the concerns raised by Po-Chedley and Fu (2012).

b. AMSU calibration

The pre-launch characterization of the AMSU instruments was more extensive than the MSU, and its design more advanced, so we used the calibration procedure recommended in the *NOAA KLM Users Guide* (Robel and Graumann, 2014). We have seen no clear evidence that the resulting calibrated T_b have a dependence on the AMSU instrument temperature, as was found with the MSU (e.g. Fig. 3).

4. MSU and AMSU Tb grid generation

The initial step in T_b grid generation at the reference Earth incidence angle (s) is to create monthly grids of the separate MSU2, 3, 4, and AMSU5, 7, 9 at their separate view angles. For the MSU, which has 11 footprints, there are 6 view angles corresponding to footprints 1 and 11, 2 and 10, *etc*. For the AMSU the 30 footprints cover 15 separate view angles. For MSU, these are binned at 1 deg. latitude/longitude resolution, with each T_b being "smeared" over 3 × 3 1 deg. gridpoints (due

Table 1. Instrument body temperature calibration regression coefficients (β) used in the MSU T_b calibration procedure.

Satellite	Orbit	MSU2 β	MSU3 β	MSU4 β	Basis
Tiros-N	1:30	0.046	0.062	0.024	Average of other 1:30 satellite results
NOAA-6	7:30	0.038	0.054	0.045	Avg. of overlaps vs. NOAA-7 and NOAA-9
NOAA-7	1:30	0.048	0.091	0.032	Avg. of overlaps vs. NOAA-6 and NOAA-8
NOAA-8	7:30	0.057	0.059	0.039	Overlap vs. NOAA-7
NOAA-9	1:30	0.032	0.062	0.024	Overlap vs. NOAA-6
NOAA-10	7:30	0.029	0.026	0.045	Overlap vs. NOAA-11
NOAA-11	1:30	0.059	0.060	0.017	Overlap vs. NOAA-12
NOAA-12	7:30	0.032	0.041	0.031	Overlap vs. NOAA-11
NOAA-14	1:30	0.046	0.035	0.022	Overlap vs. NOAA-12

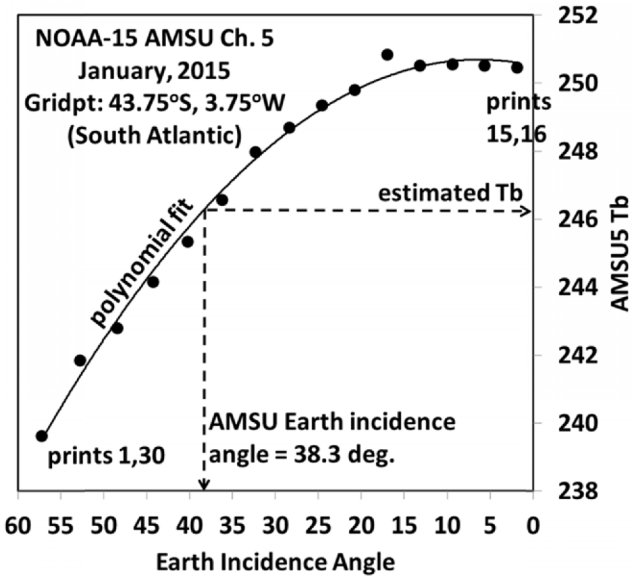

Fig. 4. An example of the second order polynomial estimation of a gridpoint monthly average T_b at the desired reference Earth incidence angle from all footprint data at that gridpoint for the month.

to sparse MSU footprint sampling), and the resulting grids are then averaged to 2.5 deg. resolution; for more densely sampled AMSU the data are averaged directly into 2.5 deg. latitude/longitude bins.

Also computed are monthly latitude-dependent averages of the Earth incidence angles corresponding to each satellite view angle based upon satellite ephemeris data available in two- line element (TLE) files, available from http://www.space-track.org. The TLE data in some months produced somewhat noisy results, especially from the older satellites, and the resulting calculations required median filtering to produce a smooth time series of Earth incidence angle.

The resulting monthly T_b gridpoint averages were then fitted as a function of Earth incidence angle with a second order polynomial. The T_b for the desired reference Earth incidence angle is then estimated from the fitted curve, rather than from the view-angle averages. An example of this fit is shown in Fig. 4, for AMSU channel 5 at a single gridpoint, month, and satellite. This new procedure has four advantages over our previous limb correction procedures. Firstly, all of the different view angle T_b measurements are included in the optimum estimation of the T_b at the desired Earth incidence angle, maximizing sampling signal-to-noise. Secondly, the resulting average calculation for a gridpoint location is based only upon data from that location, a new feature that avoids errors inherent in the old calculation of LT from geographically different areas. Thirdly, the orbit altitude decay effect (which has been large only for calculation of the old LT), as well as different satellites' altitudes, is automatically handled since we use routine satellite ephemeris updates to calculate Earth incidence angles, which are the new basis for T_b estimation, not footprint positions *per se*. Finally, working from monthly grids of separate view angle averages, as opposed to the original orbit files for earlier versions, allows rapid reprocessing of the entire satellite archive of data, allowing us to efficiently test different nominal view angles for the products, matching of the MSU and AMSU view angles, changes in diurnal drift estimation, *etc*.

5. Diurnal drift adjustment

Due to orbit decay, all of the satellites used here, except Aqua, experienced a diurnal drift in the local observation time (Fig. 1) which causes spurious cooling of the afternoon satellites' tropospheric measurements, and spurious warming of the morning satellites, primarily over land. While this might sound like a potentially large adjustment, (1) deep-layer temperature measurements are less affected by the diurnal cycle than surface temperature, and (2) to the extent the diurnal cycle in measured T_b is a perfect sinusoid and the satellite ascending and descending passes are 12 hr apart, there would be no satellite drift impact on the average T_b data. Unfortunately, the conditions in (2) are not exactly met (except the observations are indeed 12 hr apart at the equator).

Adjustment for the resulting drift in the T_b can be handled either empirically or with global climate model estimates of the diurnal cycle, the latter technique being used in the RSS dataset. Here the diurnal drift effects are empirically quantified at the gridpoint level by linearly regressing the T_b difference between NOAA-15 (a drifting 7:30 satellite) and Aqua (a non-drifting satellite) to the change in the local observation time of NOAA-15. This provides initial diurnal drift coefficients, for the twelve calendar months, for all of the 7:30 satellites. Similarly, regressions of NOAA-19 against NOAA-18 during 2009-2014, when NOAA-18 was drifting rapidly and NOAA-19 had no net drift, provided diurnal drift coefficients for the 1:30 satellites.

The resulting initial estimates of the diurnal drift coefficients (degree $^{o}C\ hr^{-1}$) for MSU2/AMSU5 at the gridpoint level were somewhat noisy and required smoothing. Since global imagery of the drift coefficients showed diurnal drift depends upon terrain altitude and the dryness of the region (deserts have stronger diurnal cycles in temperature than do rain forests), multiple linear regressions were performed within each 2.5 deg. latitude band between the initial gridpoint diurnal drift coefficients against terrain altitude, as well as against GPCP average rainfall (1981-2010) for each calendar month (Adler et al., 2003). Those regression relationships were then applied to the gridpoint average rainfall and terrain elevation within the latitude band. Over ocean, where diurnal drift effects are small, the gridpoint drift coefficients are replaced with the corresponding ocean zonal band averages of those gridpoint drift coefficients.

Figure 5 shows an example of the final diurnal drift coefficients (in degree $^{o}C\ hr^{-1}$ of ascending node time drift) used for MSU2/AMSU5 at the reference Earth incidence angle for January and June. The reason why the drift coefficients change

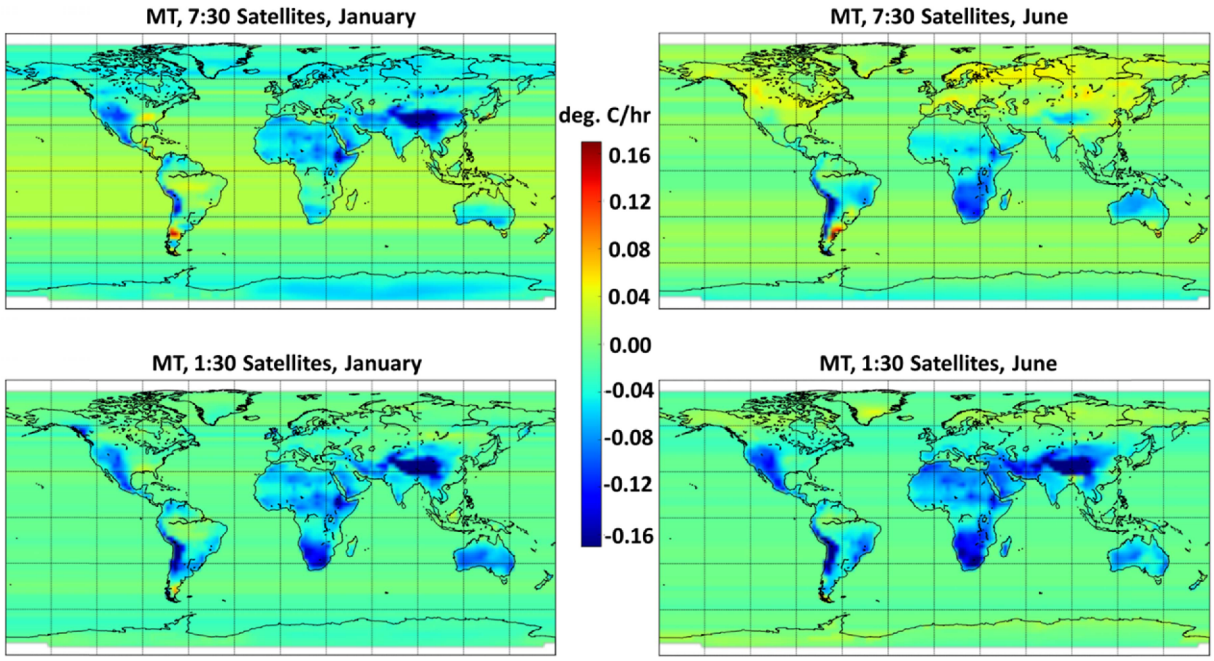

Fig. 5. Diurnal drift coefficients (degree ^{o}C hr^{-1}) for MSU2/AMSU5 for the months of January (left) and June (right) applied to the "7:30" satellites (top) and "1:30" satellites (bottom). The NASA Aqua satellite had no diurnal drift.

sign at high northern latitudes is a combination of early sunrise and late sunset time in June, and the fact that the ascending and descending orbit satellite observations at high latitudes approach the same time, instead of being 12 hours apart as they are at the equator.

We also compute and apply diurnal drift coefficients for MSU channels 3 and 4 (AMSU channels 7 and 9), but the drifts and resulting adjustments are very small.

6. Product anomaly calculation

The calculation of the monthly gridpoint anomalies that are the basis for the UAH Version 6 products is a multi-step process, and is based upon the diurnally adjusted T_b grids at the reference Earth incidence angle (s) addressed up to this point.

First, we compute initial monthly gridpoint anomalies for all morning satellites versus the NOAA-10 annual cycle, and for all afternoon satellites versus the NOAA-11 annual cycle, using only the NOAA-10/NOAA-11 overlap period for the annual cycle calculation.

Next, we apply a trend adjustment of NOAA-11 relative to NOAA-10 and NOAA-12, and another trend adjustment of NOAA-14 relative to NOAA-12 and NOAA-15. These force an average match between the middle satellite's trends to the bounding satellites' trends during their mutual overlap periods.

Then inter-satellite relative biases are calculated and removed. These are cumulative and are calculated in the following order: Tiros-N vs. NOAA-6; NOAA-7 vs. NOAA-6; NOAA-9 vs. NOAA-6; NOAA-8 vs. NOAA-7; NOAA-10 vs. NOAA-9; NOAA-11 vs. NOAA-10; NOAA-12 vs. NOAA-11; NOAA-14 vs. NOAA-12; NOAA-15 vs. NOAA-14; Aqua vs. NOAA-15; NOAA-18 vs. Aqua; NOAA-19 vs. NOAA-18. When multiple satellites are operating in the same months, their satellite gridpoint anomalies are averaged together.

The intercalibrated and trend-adjusted data are then used to compute residual gridpoint anomaly annual cycles, which are smoothed with a four-term Fourier series. Those smoothed gridpoint cycles are then removed from the anomalies.

Next, an MSU channel 3 calibration drift correction is applied, using global averages linearly interpolated between the following values: +0.70 deg. ^{o}C (Dec. 1978); +0.70 deg. ^{o}C (Dec. 1979); +0.08 deg. ^{o}C (Dec. 1980); –0.11 deg. ^{o}C (Dec. 1982); 0.00 deg. ^{o}C (Dec. 2002). These corrections were based upon an initial global dataset of MSU2, 3, and 4 anomalies to make the MSU3 anomalies very early in the satellite record have approximately the same relationship they had to the MSU2 and MSU4 anomalies later in the record. More detail regarding this calibration drift correction is included in Section 7.

LT anomaly grids were then created from the MSU2,3,4 grids and the AMSU5,7,9 grids using Eq. 1.

The ocean and land anomalies for MT, LT, TP and LS were smoothed in longitude with a [1,1,1,1,1] filter, with only land data being used for smoothed land gridpoints, and only ocean data used for smoothed ocean gridpoints. Thus, near-coastal locations in general had fewer than five gridpoints included in their smoothing.

Finally, the remaining residual annual cycle was computed and removed from gridpoint anomalies, relative to 1981-2010 base period. The final MT, LT, TP, and LS product files are then saved.

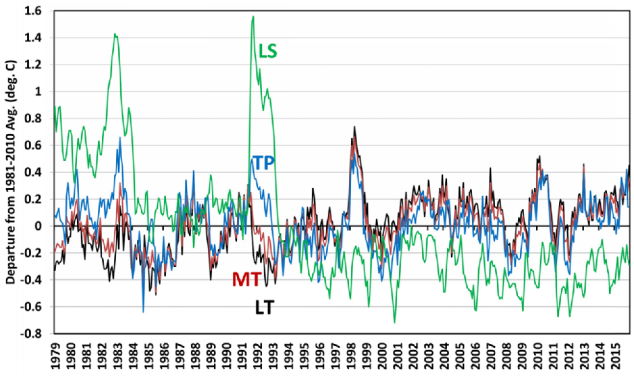

Fig. 6. Monthly global-average temperature variations for the lower troposphere (black), mid-troposphere (red), tropopause level (blue), and lower stratosphere (green), January 1979 through December 2015.

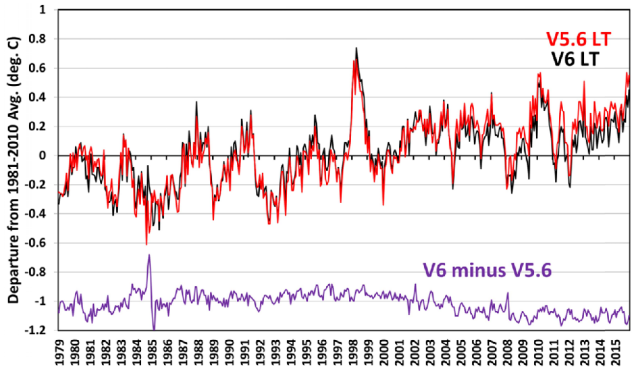

Fig. 7. Monthly global-average temperature anomalies for the lower troposphere from January 1979 through December, 2015 for the old and new versions of LT, and their difference (offset by 1 deg. °C).

7. Sample results and discussion

a. Global average results

The resulting time series of global average MT (mid-troposphere, from MSU2/AMSU5), TP (our new tropopause level product, from MSU3/AMSU7), LS (lower stratosphere, from MSU4/AMSU9), and LT (a linear combination of MT, TP, and LS) anomalies are shown in Fig. 6. LT has the warmest trend of the products (+0.11°C decade^{-1}), with the MT trend (+0.07°C decade^{-1}) being slightly weaker due to strong cooling in the lower stratosphere (LS, −0.31°C decade^{-1}). The TP trend is slightly negative (−0.01°C decade^{-1}) since that channel is centered near the tropopause and so is influenced by lower stratospheric cooling as well as tropospheric warming.

The global average LT anomalies for the new and old versions are shown in Fig. 7. Note that in the early part of the record, Version 6 has somewhat faster warming than in Version 5.6, but then the latter part of the record has reduced (or even eliminated) warming, producing results closer to the behavior of the RSS LT dataset. This is partly due to our new diurnal drift adjustment, especially for the NOAA-15 satellite.

Since the new LT product depends upon MSU3, which had calibration drift problems early in the MSU record, some additional discussion of that correction is warranted. This drift, especially during 1980-81, was the original stated reason why a multi-channel retrieval method was not implemented over twenty years ago to compute a lower tropospheric temperature (Spencer and Christy, 1992b). The new correction is made based upon linear regression of global monthly anomalies of MSU3/AMSU7 data against MSU2/AMSU5 and MSU4/AMSU9 during 1982 through 1993 (a 12-year period exhibiting two large volcanic eruptions with differential responses in the different altitude channels). We then apply the resulting regression relationship to the entire 1979-2015 period to estimate MSU3 (AMSU7) from MSU2,4 (AMSU5,9), and compare it to the raw intercalibrated global MSU3/AMSU7 time series. A difference time series of the regression estimated and the observed MSU3/AMSU7 time series is fitted with a piecewise linear estimator to give a time series of adjustments which are then applied to the MSU3/AMSU7 monthly anomaly fields. The resulting corrections cause a few hundredths of a degree per decade increase in the MSU3/AMSU7 trend (1979-2015), and according to Eq. 1 less than a 0.02 deg. °C decade^{-1} decrease in the LT trend compared to the case where MSU3 is not corrected for this calibration drift.

Even though the old and new LT weighting profiles are significantly different, we see from Fig. 2 that application of those weighting functions to the radiosonde trend profiles (average of the RAOBCORE and RATPAC trend profiles, 1979-2014) leads to almost identical trends (+0.11°C decade^{-1}). These trends are also a good match to our new satellite-based LT trend, +0.11°C decade^{-1}, providing mutual support for the Version 6 satellite and radiosonde-based trends.

We note that the new LT weighting function is less sensitive to direct thermal emission by the land surface (17% for the new LT versus 27% for the old LT), and we calculate that a portion (0.01°C decade^{-1}) of the reduction in the global LT trend versus UAH Version 5.6 is due to less direct sensitivity to the enhanced warming of global average land areas. The same effect does not occur over the ocean because all of these channels' microwave frequencies are not directly sensitive to changes in SST since ocean microwave emissivity decreases just enough with increasing SST that the two effects cancel. This effect likely also causes a slight enhancement of the land-vs-ocean trend differences. Thus, over ocean the satellite measures a true atmosphere-only temperature trend, but over land it is mostly atmospheric with a small (17%, on average) influence from the surface. One might argue that a resulting advantage of the new LT is lesser sensitivity to long-term changes in land surface microwave emissivity, which are largely unknown.

The rest of the reduction in the LT trend between Versions 6.0 and 5.6 (−0.02°C decade^{-1}) is believed to be partly due to a

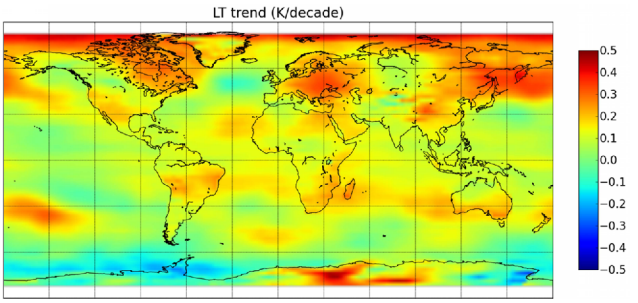

Fig. 8. Version 6 gridpoint LT temperature trends, December 1978 through January 2016.

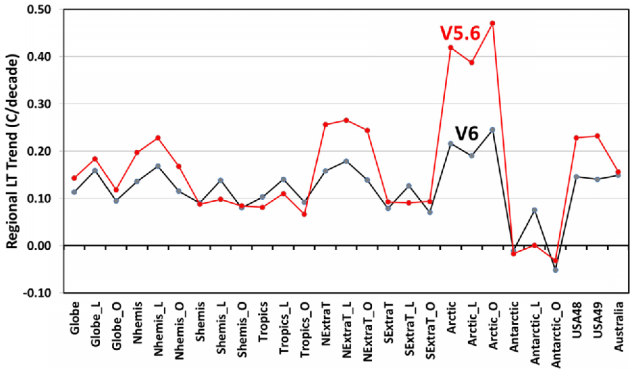

Fig. 9. Regional lower tropospheric (LT) temperature trends in Versions 6.0 and 5.6. "L" and "O" represent land and ocean, respectively.

more robust method of LT calculation, and the new diurnal drift adjustment procedure. The difference between the Version 5.6 and Version 6 trends is within our previously stated estimated error bars on the global temperature trend (+/– 0.04°C decade^{-1}). While all adjustments performed to produce the temperature products have inherent uncertainty, through sensitivity experiments we find it is difficult to obtain a global LT trend substantially greater than +0.11°C decade^{-1} without making assumptions that cannot be easily justified.

b. Gridpoint and regional results

The corresponding gridpoint trends in LT are shown in Fig. 8 for the period 1979-2015. Version 6 has inherently higher spatial resolution than the Version 5 product, which had strong spatial smoothing as part of the data processing and through the nature of how LT was calculated. The gridpoint trend map shows how the land areas, in general, have warmed faster than the ocean areas. We obtain land and ocean trends of +0.16 and +0.10°C decade^{-1}, respectively. These are somewhat weaker than thermometer-based warming trends, e.g. +0.26 for land (from CRUTem4, 1979-2014) and +0.12°C decade^{-1} for ocean (from HadSST3, 1979-2014).

The gridpoint trends for LT in Fig. 8 are not easy to measure accurately over land, primarily due to (1) the diurnal drift effect, which can be at least as large as any real temperature trends, and (2) how LT is computed, which in the old LT methodology required data from different view angles, and thus different geographic locations which can be from different air masses and over different surfaces (e.g. land and ocean). The land vs. ocean trends are very sensitive to how the difference in atmospheric weighting function height is handled between MSU channel 2 early in the record, and AMSU channel 5 later in the record (starting August, 1998). In brief, the lower in altitude the weighting function senses, the greater the brightness temperature difference between land and ocean, mostly because land microwave emissivity is approximately 0.90-0.95, while the ocean emissivity is only about 0.50 at these frequencies. As a result, if the AMSU channel 5 view angle chosen to match MSU channel 2 is too low in altitude, the net effect after satellite intercalibration will be a spurious warming of land areas and spurious cooling of ocean areas (at least when intercalibration is performed with land and ocean data combined, as done here). We were careful to match the MSU and AMSU weighting function altitudes based upon radiative transfer theory, and are reasonably confident that most of the remaining land-vs-ocean effects in the above map are real, that is, the land areas have warmed faster than the ocean regions. This is consistent with thermometer datasets of surface temperature, although our warming trends are weaker in magnitude.

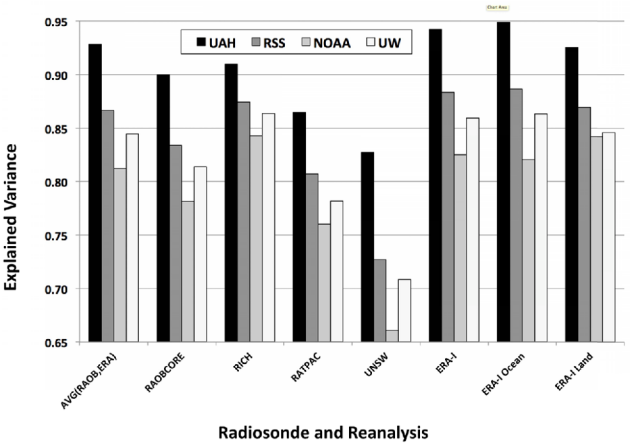

Fig. 10. Explained variance between four satellite microwave temperature datasets and various radiosonde and reanalysis datasets for yearly anomalies, 1979-2015, in mid-tropospheric temperature (MT). Radiosonde datasets and reanalyses are on the horizontal axis with each satellite temperature dataset individually represented by the vertical bars.

Changes in regional temperature trends from Version 5.6 to 6.0 are shown in Fig. 9. The largest changes are seen in the Northern Hemisphere extratropics. Trends increased a little in the tropics and over Southern Hemisphere land. Near-zero trends exist in the region around Antarctica. Future changes to Version 6, probably minor, can be expected as we refine the gridpoint diurnal drift adjustments and other aspects of our new processing strategy.

Table 2. Sources of data used in Fig. 10.

Dataset Name	Type	Citation
UAH Version 6.0	Satellite	This paper
RSS v3.3	Satellite	Mears et al., 2012
NOAA STAR v3.0	Satellite	Zou and Wang, 2011
UW v1.0	Satellite	Po-Chedley et al., 2015
HadAT2 (1979-2012)	Radiosonde	Titchner et al., 2009
RAOBCORE v1.5	Radiosonde	Haimberger et al., 2012
RICH v1.5	Radiosonde	Haimberger et al., 2012
RATPAC	Radiosonde	Free et al., 2005
UNSW	Radiosonde	Sherwood and Nishant, 2015
ERA-Interim	Reanalysis	Dee et al., 2011

c. Radiosonde comparisons

We made comparisons between satellite- and radiosonde-based estimates of temperature variability in the tropical (20°S-20°N) troposphere where climate changes are expected to be the most clearly discernable. In Fig. 10, the fraction of variance held in common is shown between four microwave-based satellite temperature datasets of the MT product and five radiosonde datasets as well as the European Centre Reanalyses (ERA-I) for tropical-average temperatures identified in Table 2, for yearly average anomalies, 1979-2015. These statistics indicate the UAH Version 6 explains slightly more variance in the independently-constructed radiosonde datasets than do other satellite-based datasets.

Of course, all datasets require adjustments, and there are other comparison studies (different time periods, time scales, and regions) that may indicate different results. This particular comparison is designed to give information on the level of agreement over a wide region for a particularly important part of the climate system, the tropical troposphere.

8. Summary and conclusions

Version 6 of the UAH MSU/AMSU global satellite temperature dataset includes substantial changes in methods and procedures from previous versions. Compared to Version 5.6, the global-average lower tropospheric temperature (LT) trend is reduced from +0.14°C decade^{-1} to +0.11°C decade^{-1} (Jan. 1979 through Dec. 2015), within our previously stated margin of error (+/– 0.04°C decade^{-1}).

We now have more confidence in the geographic distribution of the LT trends, which have inherently higher spatial resolution than previous versions, owing to a new method for computing LT that uses only data from a given gridpoint to compute LT at that gridpoint. While the new LT weighting function has slightly more sensitivity to lower stratospheric cooling, it is even more sensitive to enhanced upper tropospheric warming, which according to radiosonde-based calculations cancels out the stratospheric cooling effect on the final trend.

We have described the major changes in processing strategy, including a new method for monthly gridpoint averaging which uses all of the footprint data at the various view angles, yet eliminates the need for limb correction; a new multi-channel (rather than multi-angle) method for computing the lower tropospheric temperature product which requires an additional tropopause channel to be used; and a new empirical method for diurnal drift correction.

In addition to the lower tropospheric temperature, the mid-troposphere (from MSU2/AMSU5), and lower stratosphere (from MSU4/AMSU9) are similarly reprocessed, and a new tropopause channel (TP, from MSU3/AMSU7) is used in the LT calculation.

Radiosonde and reanalysis comparisons to this and three other published satellite microwave temperature datasets for the tropical mid-troposphere indicate somewhat better agreement for our annual anomalies, 1979-2015, although comparisons in other regions might reveal different results.

Acknowledgements. This research was supported by U.S. Department of Energy contract DE-SC0012638.

Edited by: Jhoon Kim

References

Adler, R. F., and Coauthors, 2003: The version 2 global precipitation climatology project (GPCP) monthly precipitation analysis (1979-Present). *J. Hydrometeorol.,* **4**, 1147-1167, doi:10.1175/1525-7541(2003)004<1147:TVGPCP>2.0.CO;2.

Christy, J. R., R. W. Spencer, and W. D. Braswell, 2000: MSU tropospheric temperatures: Dataset construction and radiosonde comparisons. *J. Atmos. Ocean. Tech.*, **17**, 1153-1170, doi:10.1175/1520-0426(2000)017<1153:MTTDCA>2.0.CO;2.

Conrath, B. J., 1972: Vertical resolution of temperature profiles obtained from remote radiation measurements. *J. Atmos. Sci.,* **29**, 1262-1271, doi:10.1175/1520-0469(1972)029<1262:VROTPO>2.0.CO;2.

Dee, D. P., and Coauthors, 2011: The ERA-Interim reanalysis: configuration and performance of the data assimilation system. *Quart. J. Roy. Meteor. Soc*., **137**, 553-597, doi:10.1002/qj.828.

Free, M., and D. J. Seidel, 2005: Causes of differing temperature trends in radiosonde upper air datasets. *J. Geophys. Res*., **110**, D07101, doi:10.1029/2004JD005481.

_____, _____, J. K. Angell, J. Lanzante, I. Durre, and T. C. Peterson, 2005: Radiosonde Atmospheric Temperature Products for Assessing Climate (RATPAC): A new data set of large-area anomaly time series. *J. Geophys. Res*., **110**, D22101, doi:10.1029/2005JD006169.

Fu, Q., C. M. Johanson, S. G. Warren, and D. J. Seidel, 2004: Contribution of stratospheric cooling to satellite-inferred tropospheric temperature trends. *Nature*, **429**, 55-58, doi:10.1038/nature02524.

Haimberger, L., 2007: Homogenization of radiosonde temperature time series using innovation statistics. *J. Climate*, **20**, 1377-1403, doi:10.1175/JCLI4050.1.

Haimberger, L., C. Tavolato, and S. Sperka, 2012: Homogenization of the global radiosonde temperature dataset through combined comparison with reanalysis background series and neighboring stations. *J. Climate,* **25**, 8108-8131, doi:10.1175/JCLI-D-11-00668.1.

Lu, Q., and W. Bell, 2014: Characterizing channel center frequencies in AMSU-A and MSU Microwave Sounding Instruments. *J. Atmos.*

Ocean. Tech., **31**, 1713-1732, doi:10.1175/JTECH-D-13-00136.1.

Mears, C. A., M. C. Schabel, and F. J. Wentz, 2003: A reanalysis of the MSU channel 2 tropospheric temperature record. *J. Climate*, **16**, 3650-3664, doi:10.1175/1520-0442(2003)016<3650:AROTMC>2.0.CO;2.

_____, F. J. Wentz, and P. W. Thorne, 2012: Assessing the value of Microwave Sounding Unit radiosonde comparisons in ascertaining errors in climate data records of tropospheric temperatures. *J. Geophys. Res.*, **117**, D19103, doi:10.1029/2012JD017710.

Robel, J., and A. Graumann, 2014: NOAA KLM User's Guide with NOAA-N, N Prime, and Metop Supplements. NOAA/NESDIS/NCDC, Asheville, NC, 2530 pp.

Po-Chedley, S., and Q. Fu, 2012: A bias in the midtropospheric channel warm target factor on the NOAA-9 Microwave Sounding Unit. *J. Atmos. Ocean. Tech.*, **29**, 646-652, doi:10.1175/JTECH-D-11-00147.1.

_____, T. J. Thorsen, and Q. Fu, 2015: Removing diurnal cycle contamination in satellite-derived tropospheric temperatures: Understanding tropical tropospheric trend discrepancies. *J. Climate*, **28**, 2274-2290, doi:10.1175/JCLI-D-13-00767.1.

Sherwood, S. C., and N. Nishant, 2015: Atmospheric changes through 2012 as shown by iteratively homogenised radiosonde temperature and wind data (IUKv2). *Env. Res. Lett.*, **10**, 054007, doi:10.1088/1748-9326/10/5/054007.

Spencer, R. W., and J. R. Christy, 1990: Precise monitoring of global temperature trends from satellites. *Science*, **247**, 1558-1562, doi:10.1126/science.247.4950.1558.

_____, and _____, 1992a: Precision and radiosonde validation of satellite gridpoint temperature anomalies, Part I: MSU channel 2. *J. Climate*, **5**, 847-857, doi:10.1175/1520-0442(1992)005<0847:PARVOS>2.0.CO;2.

_____, and _____, 1992b: Precision and radiosonde validation of satellite gridpoint temperature anomalies, Part II: A tropospheric retrieval and trends during 1979-90. *J. Climate*, **5**, 858-866, doi:10.1175/1520-0442(1992)005<0858:PARVOS>2.0.CO;2.

_____, and _____, 1993: Precision lower stratospheric temperature monitoring with the MSU: Technique, validation, and results 1979-91. *J. Climate*, **6**, 1301-1326, doi:10.1175/1520-0442(1993)006<1194:PLSTMW>2.0.CO;2.

Titchner, H. A., P. W. Thorne, M. P. McCarthy, S. F. B. Tett, L. Haimberger, and D. E. Parker, 2009: Critically reassessing tropospheric temperature trends from radiosondes using realistic validation experiments. *J. Climate*, **22**, 465-485, doi:10.1175/2008JCLI2419.1.

Wentz, F. J., and M. Schabel, 1998: Effects of orbit decay on satellite-derived lower-tropospheric temperature trends. *Nature*, **394**, 661-664, doi:10.1038/29267.

Zou, C.-Z., and W. Wang, 2011: Inter-satellite calibration of AMSU-A observations for weather and climate applications. *J. Geophys. Res.*, **116**, D23113, doi:10.1029/2011JD016205.